Radiation-Effects Testing for the National Ignition Facility Final Optics

C. D. Marshall *S. A. Payne*

J. A. Speth *M. Borden**

L. D. DeLoach *S. Karr***

Introduction

The principal technical goal of the National Ignition Facility (NIF) is to achieve thermonuclear ignition in a laboratory environment by means of inertial confinement fusion (ICF). Such ignition will enable the NIF to service the Department of Energy Stockpile Stewardship Management Program, to achieve inertial fusion energy goals, and to advance scientific frontiers.[1] All three applications will make use of the extreme conditions created in the target chamber. For a predicted 20-MJ yield scenario, the NIF will produce ~10^{19} neutrons with a characteristic deuterium–tritium (D–T) fusion energy of 14 MeV per neutron. The ICF process will also directly or indirectly produce x rays, gamma rays, secondary neutrons, and solid, liquid, and gaseous target debris. Thus, a critical design issue is protecting the final optical components and sophisticated target diagnostics in the harsh environment.

Figure 1 shows the basic geometry of the NIF target chamber. The final optics package is located 6.5 m from the target and chamber center. The debris shields, which are designed to absorb x rays and target debris, are likely to require frequent replacement. The target chamber wall, ~1-m-thick concrete shielding, and target area concrete shield wall (not shown in Fig. 1) will absorb virtually all of the radiation and target debris and protect most of the laser system from direct line-of-sight irradiation. However, penetrating radiation, such as neutrons and gamma rays, will propagate through the ~1-cm-thick debris shields to interact with the relatively expensive fused-silica focus lenses and potassium-dihydrogen-phosphate (KDP) frequency-conversion crystals.

This article focuses on potential degradation of the NIF final-focus lenses and frequency-conversion crystals, which must last for many years. Furthermore, an ICF-based power plant may become possible in the next century, when it will likely be necessary to maintain SiO_2 final optics at an elevated temperature to anneal the radiation-induced defects that are formed.[2]

Review of Fundamentals

Fused silica (synthetic SiO_2) or fused quartz (natural SiO_2) are among the optical materials of choice for situations involving ultraviolet transparency, precision quality, large size, or harsh environments. Issues surrounding the radiation hardness of SiO_2 have been studied for many decades,[3–6] and the recent emergence

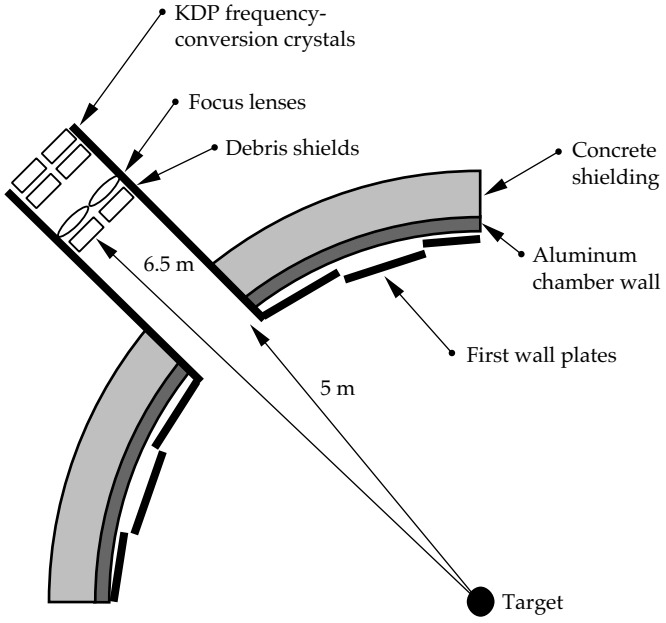

FIGURE 1. Geometry of the NIF target chamber and position of the final optical components. (50-02-0694-2720pb02)

*Los Alamos National Laboratory, Los Alamos, New Mexico.
**Sandia National Laboratory, Albuquerque, New Mexico.

of deep-ultraviolet (DUV) lithography has prompted renewed interest.[7–9] Many defects have been characterized and elucidated, and this report builds on that foundation.[3–6] However, substantial uncertainty remains in the literature, partly as a consequence of the often unclearly specified radiation conditions and different types of SiO_2 that have been used. We tested a wide variety of commercial fused silica and fused quartz samples with a wide variety of specified irradiation conditions, leading to an improved understanding of the issues important for SiO_2 radiation hardness.

Far less is known about the radiation resistance of KDP.[10,11] Our work is intended to assess radiation hardness and to unravel some of the basic material physics issues when SiO_2 and KDP encounter gamma-ray or neutron irradiation.[12]

In general, when electromagnetic radiation of sufficient energy is used to irradiate an optical material, solarization or optical darkening occurs. Absorption or scattering of photons leads to the generation of energetic electrons and holes that eventually react with pre-existing structural defects (precursors) or the intrinsic material itself to create the electronic defects associated with solarization.[5,13]

A ~1-MeV gamma ray, typical of the energy range to be produced on the NIF, is, in principle, capable of yielding about 10^5 electron–hole (e–h) pairs per photon. The process begins by the production of energetic Compton electrons, which produce secondary electrons and e–h pairs. The action of neutrons differs from that of gamma-ray photons because of their uncharged nature. Neutrons initially collide with nuclei and can induce nuclear reactions that produce other types of radiation, such as gamma rays and alpha particles. However, some momentum transfer always occurs. The resulting "knock-on-collision" displacement damage can lead to precursor sites that later encounter electrons and holes and become converted to other types of defects. Precursors can also result from manufacturing processes, including oxidizing or reducing conditions.

Many different defects can be created in irradiated SiO_2 and KDP. Here, we review those most prominently observed in our studies. In perfect SiO_2 glass, silicon is tetrahedrally bonded by four oxygens in a continuous, random glass network. The Si–O–Si bonds can be strained, which is believed to render the site more susceptible to electronically induced displacements.[14] An oxygen-deficient center (ODC), which gives rise to an absorption band at 5 eV can be created as a result of collisions with neutrons.[15] The ODC can be converted to an E' defect center by losing an electron.[5,16,17] The E' absorption occurs at 5.8 eV. The precise absorption spectra associated with all defect species have not yet been fully resolved. For example, the B_1 band, with an absorption at 4 eV, is only observed in fused quartz, and a definitive defect site has not been correlated with this band.[5,15] An Al impurity[15,18] is known to give rise to absorption at 2.0 eV. We found evidence of the Al impurity, B_1, D_0, and E' absorption bands during our work as a result of gamma-ray electronic excitations, and we believe that neutron collisions produce the ODC.

Many different absorption bands have been identified with impurities and gamma-ray irradiation in KDP. For example, transition metals, such as Al, Fe, As, Cr, Pb, and V, can lead to significant radiation-induced absorption in KDP, all with absorptions in various portions of the ultraviolet spectrum. In general, these absorptions arise from electrons that are promoted by means of irradiation to the KDP conduction band in ways similar to those described above for SiO_2. The electrons are then trapped at impurity sites in the band gap between the conduction and valence band. The energy gap between the impurity site and the lower edge of the conduction band determines the wavelength of induced absorption.

Penetrating Radiation Characteristics

NIF

Most of the penetrating radiation from the NIF target will emanate directly from 14-MeV monochromatic neutrons (the flux of 17.6-MeV gamma rays from D–T fusion is less by a factor of 10^4). However, significant neutron-induced nuclear reactions will also arise from various structures in the target area.[19] These secondary reactions produce penetrating radiation consisting of neutrons that range from $<<0.01$ to ~10 MeV in energy, and gamma rays that range from 0.01 to 10 MeV. Depending on whether the radiation is prompt (directly from the target) or secondary, the pulse duration is in the range of 5 to 100 ns, respectively.

The time-integrated dose over an expected 30-year lifetime of the NIF is expected to be 1.1 Mrad from neutrons (n^o) and 0.6 Mrad from gamma rays in the SiO_2 focus lenses; in KDP, the time-integrated dose is 1.1 Mrad from n^o and 0.5 Mrad from gamma rays. These doses correspond to ~2 and ~1 krad of n^o and gamma rays, respectively, for each of the 20-MJ yield shots with a total 385-MJ/year yield.[19] For reference, 1 rad is defined as 10^{-5} J of absorbed energy per gram of material. Of course, variations in both the transverse and longitudinal doses arise from absorption and shadowing, but the ±10% variation is not significant compared to other issues, such as the NIF gain and shot rate, which may be accelerated.

Sources for Radiation Testing

No radiation test sources currently in operation can produce the necessary spectrum and temporal format of neutrons and gamma rays that is exactly equivalent for direct accelerated life tests of the NIF final optics.

Thus, we used a variety of radiation sources that bracket the problem to interpolate results and predict what will happen on the NIF. Table 1 lists the radiation sources we used and their relevant temporal and spectral characteristics. Modeling exercises benchmarked against the accumulated data provided a realistic view of the radiation damage to optics that may be expected from the NIF.

The Los Alamos Neutron Science Center (LANSCE) shown in Fig. 2 is a kilometer-long, proton-accelerator, neutron-spallation source that provides a hard neutron and gamma-ray spectrum extending from thermal energies <<0.01 MeV to several hundred MeV. The pulse format of the accelerator furnishes a long (ms) train of 300-ps pulses with a macrorepetition rate of 10 Hz. This facility allowed us to obtain both neutron and gamma-ray pulsed irradiations with energies and doses spanning the relevant range for the NIF.

The Sandia National Laboratory Pulsed Reactor facility No. III (SPR-III) shown in Fig. 3 is an enriched ^{235}U pulsed nuclear reactor that provides a relatively hard (for a reactor) neutron spectrum extending from thermal energies to ~3 MeV.[20] The reactor is nominally operated with 100-μs pulses at a repetition rate of once

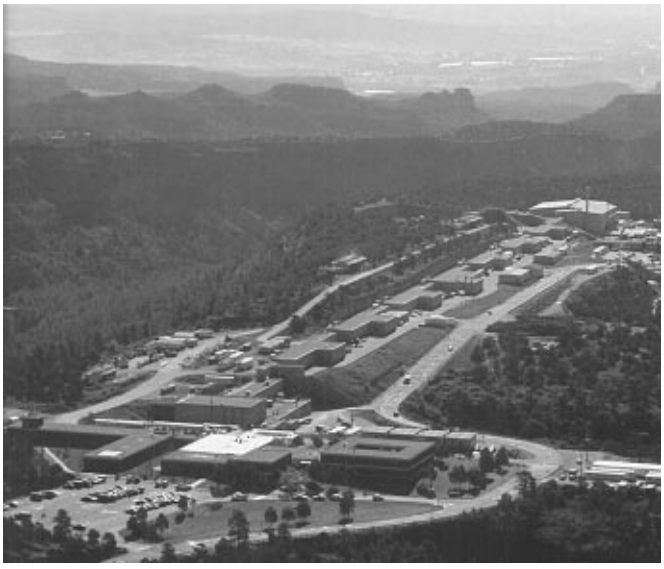

FIGURE 2. The Los Alamos Neutron Science Center (LANSCE) was the pulsed, high-energy (>10-MeV) neutron-irradiation facility used in our studies. (70-17-1095-2274pb04)

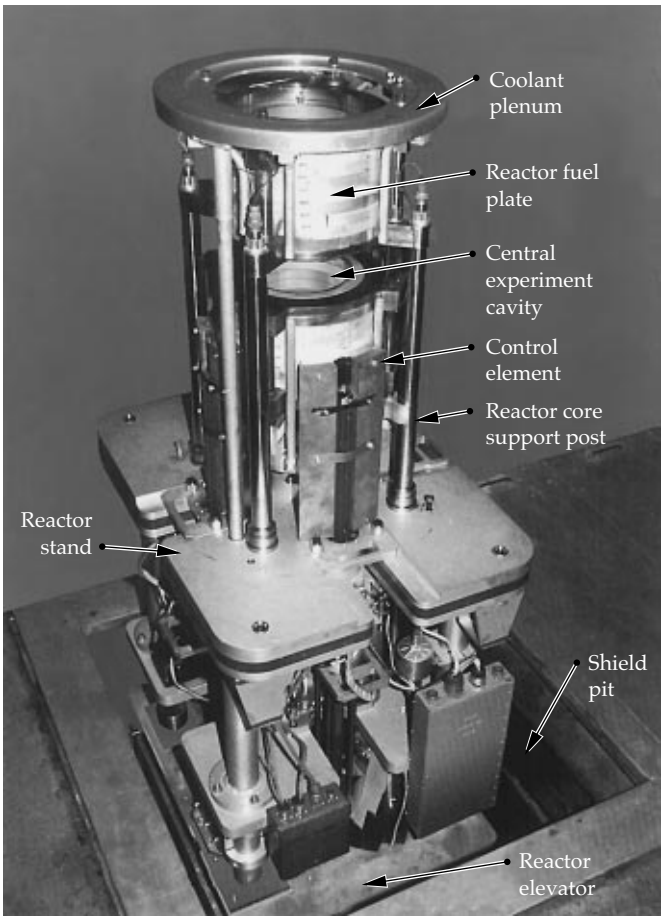

FIGURE 3. The Sandia National Laboratory Pulsed Reactor No. III (SPR-III) was the pulsed nuclear reactor used in our studies. (70-17-1095-2274pb03)

TABLE 1. Summary of radiation source characteristics that were collaboratively used for accelerated life testing of NIF final optics components at LANL, SNL, LLNL, and French Commissariat Energie Atomique Laboratories.

		NIF	LANL LANSCE	SNL SPR-III	LLNL RTNS-II	CEA Sames	LLNL ^{60}Co	LLNL e^- LINAC
Neutrons	Spectra (MeV)	14 primary <0.01–1 low dose	<0.01–100	<0.01–1	14	14	None	None
	Pulse format	5 ns	ps trains	100 μs	continuous (or 5 ns)	continuous		
	NIF 30-yr dose (Mrad)	1	4	4	4	N/A	N/A	N/A
Gamma rays	Spectra (MeV)	0.01–10	1–100	0.01–1	0.01 to 1	0.01 to 1	1	0.01–50
	Pulse format	20 ns	ps trains	100 μs	continuous	continuous	continuous	20 ns
	NIF 30-yr dose (MRad)	0.5	4	4	N/A	N/A	4	4

every 2 hr. The neutron energy spectrum is peaked at 1 MeV but is broad, with 99% of the neutron energy bracketed within 0.01 to 10 MeV. This facility allowed us to obtain gamma-ray irradiations with energies close to the relevant range for the NIF, along with n^o irradiation with energies near that of the NIF (see Table 1).

The French Commissariat Energie Atomique (CEA) Sames neutron source and LLNL RTNS-II neutron source are D accelerators with T targets that provided a continuous source of direct, 14-MeV, D–T fusion neutrons. These facilities provided us with the best match to the neutron energies on the NIF; however, the continuous temporal format is dissimilar. Gamma-ray irradiation is also present in these sources due to secondary reactions.

At LLNL, an electron accelerator spallation source (0.01 to 50 MeV) and a ^{60}Co source (1 MeV) also provided pure gamma-ray radiation in ns pulsed and continuous formats, respectively. These gamma-ray facilities, together with the mixed-neutron and gamma-ray sources, allowed for the separation of effects that arose from gamma rays and neutrons.

Experimental Results

We have developed a physical model of the primary radiation-damage pathways for silica glass and KDP in the penetrating radiation dose range of interest for the NIF. The primary consideration was the induced optical absorption in the glasses as a function of absorbed radiation dose. The temporal format of the radiation pulses was of interest because potential thermal annealing at room temperature could affect radiation damage of subsequent pulses. The radiation spectral shape was also of concern because neutrons of different energy have differing percentages of elastic and inelastic scattering.

We studied as many as 25 sources and grades of SiO_2 to understand the impact of manufacturing methods on precursors to damage. In addition, we studied many different impurities in deliberately doped KDP to understand the impacts of purity and process control in the starting material.

Radiation Effects in Silica Glass

Figure 4 is an example of eight types of SiO_2 we tested following irradiation, including fused silica and fused quartz from different vendors and manufacturing processes. All samples were simultaneously irradiated with 3.7 Mrad of gamma rays from a ^{60}Co source. The results varied widely.

Despite the wide variation in radiation resistance, these samples led to only four radiation-induced absorption spectral shapes, as shown in Fig. 5. From

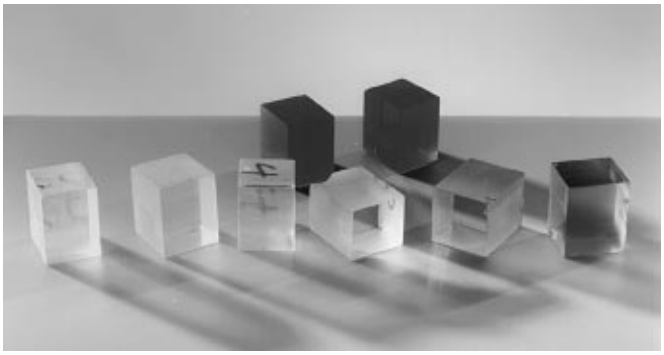

FIGURE 4. Eight different types of fused silica and fused quartz from several different manufacturers. All were irradiated with 3.7 Mrad of gamma rays from a ^{60}Co source. (70-15-1094-3620pb02)

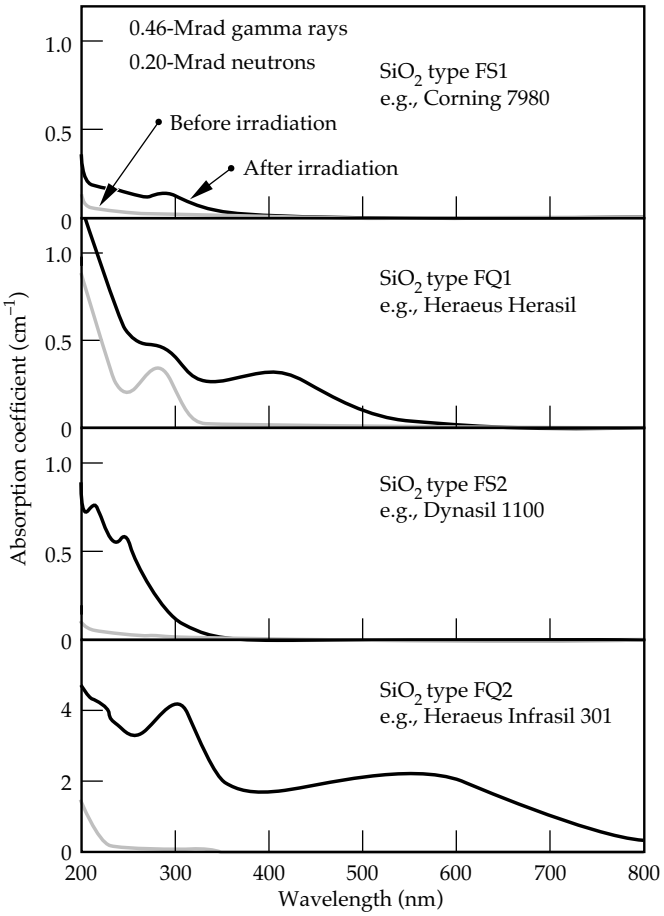

FIGURE 5. Under identical doses of 200-krad neutron and 460-krad gamma irradiation, the absorption spectra of all 25 types of SiO_2 that we studied fell into four distinct classes. (70-17-0596-1038pb01)

this information and data obtained on other radiation sources, it was possible to determine the origin of the prominent spectral shapes. The peak at 246 nm arises from direct-neutron, collision-induced displacements creating a localized ODC that is intrinsic to all SiO_2. The absorption peak at 300 nm in Fig. 5(b) arises from the conversion of 241-nm defect absorption that is present

prior to irradiation, which is likely due to a Ge impurity center originating from the manufacturing process. The peak at 210 nm (E′ defect) is due to a two-step process of first creating the 246-nm ODC defect and then converting it into an E′ center with gamma rays. The peak centered at 550 nm is most likely due to Al impurities in the SiO_2, as suggested in the literature.[5,16,17] The four spectra shown in Fig. 5 correspond to the four classes of SiO_2 in Table 2. The most radiation-hard variants are synthetic fused silicas, such as Corning 7980 and Heraeus Suprasil grades.[12]

To benchmark the effective lifetime of the NIF optics, it was necessary to use a mixed neutron and gamma-ray source because synergistic neutron and gamma pathways lead to radiation-induced damage. The SPR-III reactor was a versatile radiation source for our purposes, with 100-μs pulse operation, a mixed neutron and gamma dose ratio similar to the NIF (within a factor of 5), and a gamma spectrum very close to that of the NIF (see Table 1). The neutron spectrum from this largely unmoderated ^{235}U fission reactor, however, extends over a broad energy range, with a peak flux at 1 MeV. This is low compared to the direct D–T 14-MeV neutrons that will dominate the NIF spectrum. As a consequence, these results must be extrapolated to higher neutron energies (more damage per individual collision cascade created by a single neutron) to make NIF predictions. The SPR-III data are intended to provide insight into the impact of the gamma-ray and nº mix of radiation.

Figure 6 shows the results of a dose-dependent study on the SPR-III over two experimental days. One year on the NIF, with 385 MJ of fusion yield assumed in the NIF conceptual design report (CDR), is predicted to produce ~40 krad of neutron dose and ~20 krad of gamma-ray dose, hereafter referred to as a "NIF year." One shot on the SPR-III corresponds to one neutron NIF year and 5 gamma-ray NIF years.

Figure 6(a) shows the cumulative effect of up to eight pulses from the SPR-III for FS1 glasses, revealing absorptions at both 213 and 246 nm. On closer inspection, the E′ center at 213 nm grows at an accelerated rate compared to the 246-nm feature. This observation suggests that neutrons first create the ODCs, which are then converted to E′ centers by gamma rays. A critical test to confirm this synergistic gamma-ray/nº effect is

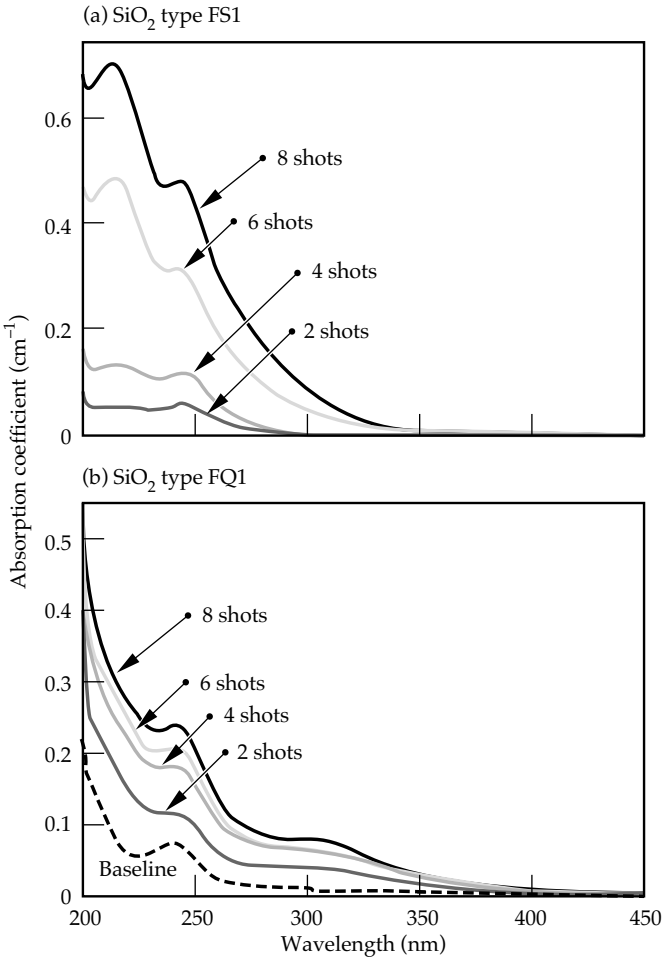

FIGURE 6. Optical absorption spectra of (a) fused silica and (b) fused quartz taken after successive shots on the SPR-III. One shot has 40 kRad nº and 100 krad of gamma-ray dose. (70-17-0596-1040pb01)

FS1 silica most rad-hard type	FS2 silica rad-soft type	FQ1 silica rad-hard type	FQ2 quartz rad-soft type
Corning 7980	Dynasil 1100	Heraeus Herasil-1top	Heraeus Infrasil-301
Corning 7940	Dynasil 1101	Heraeus Herasil-1	Dynasil QIR
Heraeus Suprasil-1		Heraeus Herasil-2	Nippon OZ
Heraeus Suprasil-2		Heraeus Herasil-3	Nippon OX1
Heraeus Suprasil-3		Heraeus Homosil	
Dynasil 4100		Heraeus Infrasil-302	
Dynasil 4101		Heraeus TO8	
Nippon ES		Dynasil QUV	
		Nippon OY	

TABLE 2. All of the SiO_2 sample types studied fell into four groupings of radiation response designated as FS1, FS2, FQ1, and FQ2, where FS = synthetic fused silica, and FQ = natural fused quartz.

shown in Fig. 7. Here the FS1-type sample is first irradiated in the SPR-III to create the ODCs, and then in a separate irradiation, it is subjected to pure gamma rays from the ^{60}Co source to show that the ODCs are converted to E′ centers. Recall that irradiation by gamma rays alone has no effect; that is, the neutrons first "soften" the material by generating ODCs.

For a pulsed radiation source, annealing of the induced defects generally follows the radiation pulse; i.e., some of the defects are self-healing at room temperature with relaxation times (inverse rate constants) ranging from nanoseconds to hours. The defects discussed in this paper are primarily long-lived defects that show no further decay after many days to months following irradiation at room temperature. The temporal format of the radiation pulse could, in general, affect the number of "permanent" defects observed, since annealable defects could be further affected by a subsequent radiation burst before they had a chance to decay. To test this possibility (i.e., to explore the dose-*rate* dependence), we performed an experiment on the SPR-III in which the radiation dose rate was varied over eight orders of magnitude. Figure 8 summarizes the results.

In the first experiment shown at the top of Fig. 8(a), the reactor was run in a steady-state mode for 30 minutes with relatively low radiation flux. In the second experiment at the bottom of Fig. 8(a), a 100-μs pulsed-neutron format was used. The total time-integrated neutron (and gamma-ray) dose during the 30-minute runs and the 100-μs pulses was measured to be approximately the same, 1.5×10^{15} n^o/cm^2 to within 10%. The neutron and gamma-ray spectra are virtually identical for these two experiments because the reactor has the same degree of moderation inside the core region. Nearly the same overall experimental time elapsed between pulses.

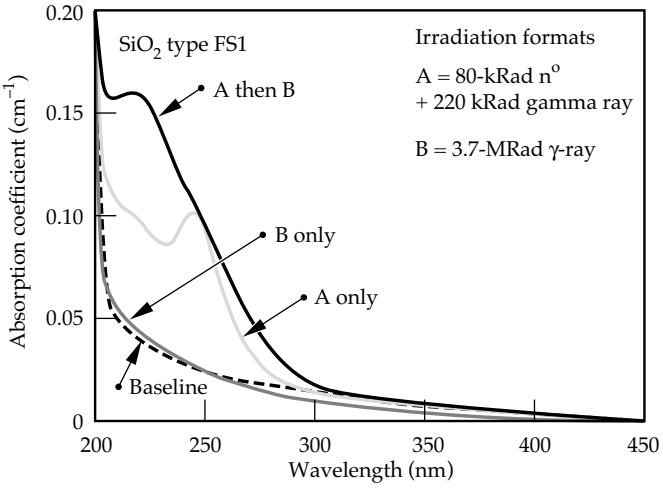

FIGURE 7. Optical absorption spectra of FS1 glass reveal that the oxygen-deficient center created by neutrons can be converted to E′ center absorption at 213 nm with gamma rays. (70-17-0596-1041pb01)

Figure 8(b) shows the results of this analysis. The data show little dose-rate dependency over the range studied in this experiment. This can be rationalized by showing that the number density of defect centers is less than the number density of atoms by four orders of magnitude. Consequently, one would expect that multiple collisions and interactions on a single physical site would be infrequent (i.e., two neutrons striking the same nucleus or damaged region) and that the system behaves as if single, isolated collisional impact sites are present.

Figure 9 is a reduction of the data in Fig. 6, which resulted from exposing fused silica and fused quartz for up to eight shots on the SPR-III reactor. The data in Fig. 7 were fit to a sum of Lorentzians, $L(\lambda)$, to account for the absorption arising from each species:

$$\alpha_i(\lambda) = \sum_i \alpha_i N_i L_i(\lambda) , \qquad (1)$$

where

$$L_i(\lambda) = \frac{\Delta\lambda_i^2}{\Delta\lambda_i^2 + (\lambda_i - \lambda)^2} \quad , \qquad (2)$$

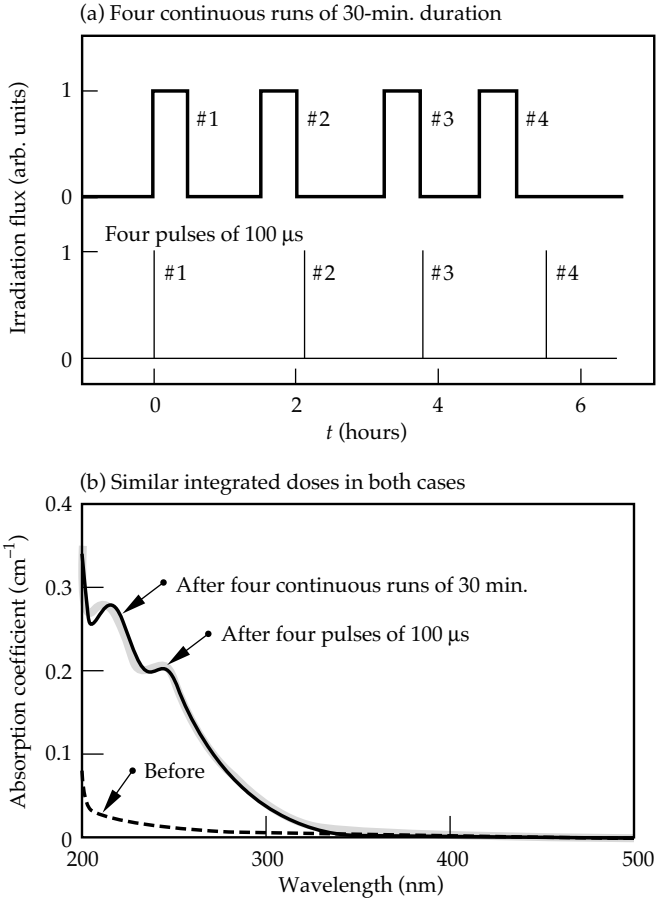

FIGURE 8. Experiment to study the effect of room-temperature annealing with short-pulse vs continuous irradiation. (a) Temporal format of radiation flux from the SPR-III. (b) The experimental results. Similar time-integrated doses were used in both experiments. (70-17-0596-1042pb01)

λ_i is the peak wavelength, and $\Delta\lambda$ is the half width at half maximum of the absorption spectrum for $i = E'$, ODC, Ge, or B_1. The data points in Fig. 9 give the peak defect absorption coefficients obtained from the Lorentzian curve fits to the spectra in Fig. 6. With fused silica, shown in Fig. 9(a), the absorption peak at 246 nm grows as a function of dose most rapidly at first; at higher doses, the 210-nm absorption peak growth rate overtakes it. This qualitative observation is consistent with the model described in Fig. 10.

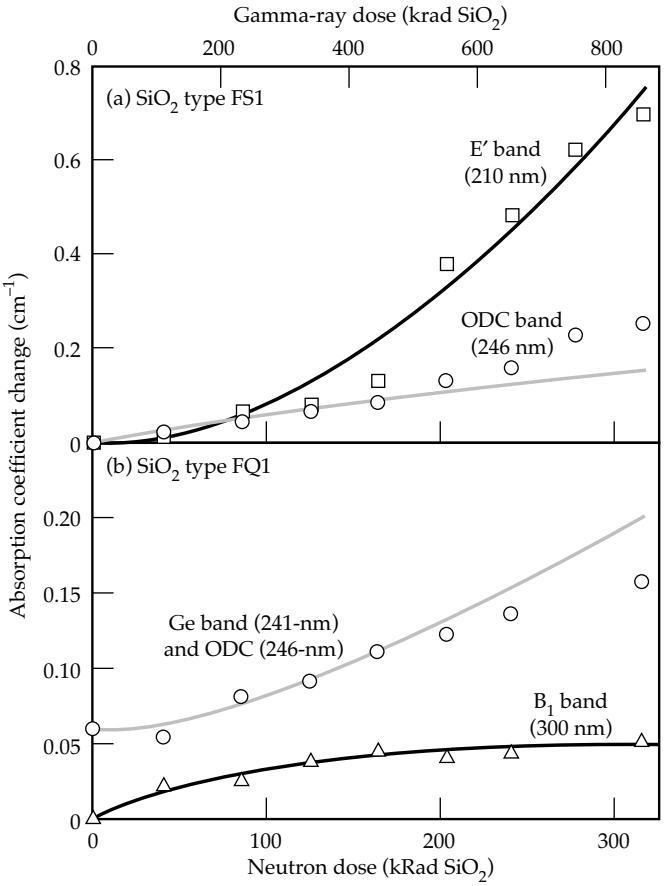

FIGURE 9. Radiation-induced absorption of E′ (210-nm), ODC (246-nm), Ge (241-nm), and B_1 (300-nm) bands in SiO_2 for (a) fused silica type FS1 and (b) fused quartz type FQ1. Data points were obtained from the SPR-III experiments. Solid lines show the numerical modeling using Eqs. (1) through (3). (70-17-0596-1043pb01)

Quantitative modeling of the defect absorption peaks shown in Fig. 9(a) for fused silica can be performed by applying rate equations derived from the model in Fig. 10 for the number density of neutron-induced ODC and subsequent gamma-ray-induced E′ defects, denoted as N_{ODC} and $N_{E'}$, respectively. The rate equations can be written as

$$\frac{dN_{ODC}}{dt} = M_{col}\sigma_{col}(E)\, N_{SiO_2}\, \frac{dF_n}{dt} - \beta_{E'}\, \frac{dD\gamma}{dt} N_{ODC} \quad (3)$$

and

$$\frac{dN_{E'}}{dt} = \beta_{E'}\, \frac{dD_\gamma}{dt} N_{ODC} \quad . \quad (4)$$

The first term in Eq. (3) describes the formation of ODC defects due to direct neutron collisions, where F_n is the neutron fluence, σ_{col} is the neutron collision cross section, N_{SiO2} is the silica number density, and M_{col} is a collision multiplier that denotes the number of cascade-collision-induced defects due to a single, primary neutron collision, as shown in the first step of Fig. 10. Equation (4) and the last term in Eq. (3) account for the second step in Fig. 10, where ODC defects are transformed into E′ defects with gamma rays. Here, $\beta_{E'}$ denotes a phenomenological conversion coefficient, and D_γ is the gamma-ray dose in krad. Defect optical absorption cross sections (σ_{ODC} and $\sigma_{E'}$) are then multiplied by the number densities obtained from Eqs. (3) and (4) to obtain the absorption coefficients in Fig. 9.

For the modeling of the defect absorption peaks in fused quartz shown in Fig. 9(b), the direct conversion of pre-existing Ge impurity into B_1 defects, with number densities N_{Ge_m} and N_{B1}, respectively, can be written as:

$$\frac{dN_{B1}}{dt} = -\frac{dN_{ODC_m}}{dt} = \beta_{B1}\, \frac{dD\gamma}{dt} N_{ODC_m} \quad , \quad (5)$$

where β_{B1} is the gamma-ray conversion coefficient. The pre-existing Ge concentration, determined from absorption spectra and mass spectra copy of individual

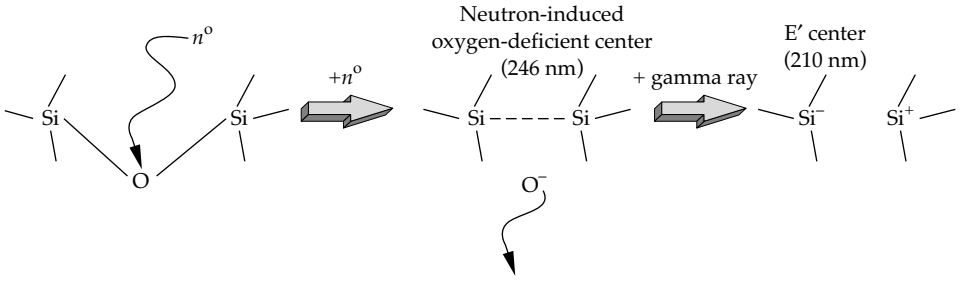

FIGURE 10. Mechanistic model of primary radiation damage mechanisms in SiO_2 that lead to changes in optical transmission. Both neutrons and gamma rays, either separately or in combination, can lead to radiation-induced damage. (70-17-0596-1039pb01)

samples, results in a nonzero initial condition. The solid lines in Fig. 9 are fits generated from Eqs. (1) through (5). Table 3 gives the parameters obtained from these curve fits.

The data-fitting parameters lead to an overdetermined system, which may not be evident from first glance at Table 3. To first order, the two unknown optical cross sections, σ_i, and the neutron multiplier, M_n, determine the height of the four curves; the two conversion coefficients, β_i, determine the shape of the data curves.

From this interpretation, the collision multiplier can be estimated by the Kinchin–Pease expression[21]

$$M_n = \frac{0.8E_{\text{dam}}}{2E_{\text{def}}}\eta_{\text{anneal}} \quad , \tag{6}$$

where E_{dam} is the average kinetic energy of the atom, which receives the initial direct collision, given as[22]

$$E_{\text{dam}} = E_n \frac{2}{A+\frac{2}{3}} \quad , \tag{7}$$

where A is the atomic mass (average of Si and two O), and $E_n \approx 1$ MeV is the neutron energy, yielding $E_{\text{dam}} \approx 0.1$ MeV. We estimate the defect formation energy of the ODC, E_{def}, as 40 eV from calculations of SiC, a related, covalently bound material.[23] An additional factor, η_{anneal}, is included by Diaz de la Rubia and others to account for the rapid (< 1-ns) annealing that occurs from the enormous local-energy deposition following a neutron–nucleus collision. Estimates from simulations place η_{anneal} at ~0.2 for fast neutrons.[21,24] Substitution into Eq. (6) yields M_n at ~200, a value that is reasonably close to our experimental assessment of 105 given the level of approximation in Eqs. (6) and (7).

To apply this model to NIF-like conditions, the neutron multiplier obtained at 1-MeV average neutron energy must be extrapolated to 14 MeV for D–T fusion neutrons present on the NIF. For this extension, we analyzed several experiments from three different high-energy neutron sources. Two experiments were performed on 14-MeV D–T fusion neutron sources (CEA Sames and LLNL RTNS-II), and one set of experiments was performed on the LANSCE high-energy (>100-MeV) proton-spallation neutron source.

Figure 11 shows the results of irradiating type FS1 fused silica (e.g. Corning 7980) with 2×10^{14} n^o/cm^2 in the Sames neutron source. The neutron multiplier, M_n, required to fit the data set was 70. The induced-absorption spectral shape is similar to that shown in Fig. 7(a) for the fission-reactor-induced absorption, indicating that no fundamentally new defects are created. The number of defects per collision is expected to be higher for 14- vs 1-MeV neutrons, however. Data taken on the RTNS-II in 1987 by Singh et al. (unpublished) at much higher doses (10^{16} n^o/cm^2) implied a neutron multiplier of 200. Data taken on the LANSCE were roughly consistent with this neutron multiplier range, although detailed dosimetry of neutron fluence as a function of neutron energy for the broad spectrum on the LANSCE is still being analyzed elsewhere. The overall spread of up to a factor of 3 in neutron-damage effectiveness (M_n) is large, depending on the experiment. The neutron multiplier inferred from these experiments varied over the range of 70 to 200, depending on the dose and

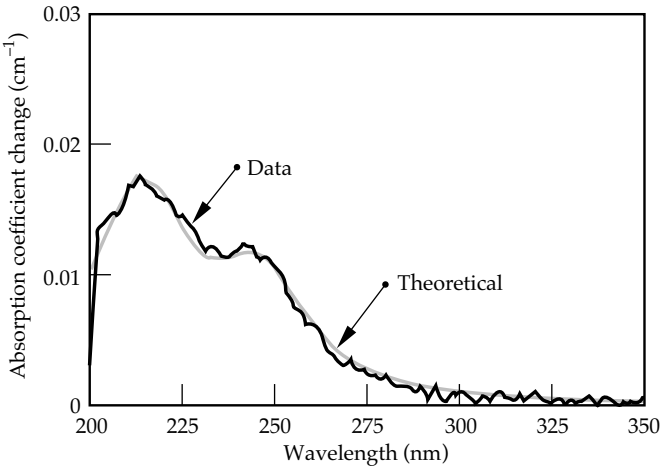

FIGURE 11. Absorption induced by the CEA Sames 14-MeV D–T fusion neutron source with 2×10^{14} n^o/cm^2 fluence at room temperature. Both data and the theoretical curve are shown. (70-17-0596-1044pb01)

TABLE 3. Parameters used to model data from the SPR-III reactor (Figs. 7–10) and to predict NIF fused silica final optics performance in Fig. 12.

Parameter	Value	Units	Source
Neutron absorption coefficient, $N_{SiO2}\sigma_{col}$	0.35	cm^{-1}	Literature
ODC to E′ gamma-ray conversion coefficient, $\beta_{E'}$	0.0007	s/krad	Data fit
Collision multiplier for 1-MeV neutrons, M_n	105	Unitless	Data fit
Collision multiplier for 14-MeV neutrons, M_n	200	Unitless	Data fit
ODC to B1 gamma-ray conversion coefficient, β_{B1}	0.004	s/krad	Data fit
Optical cross section for ODC defect, σ_{ODC}	2.1×10^{-18}	cm^2	Data fit
Optical cross section for E′ defect, $\sigma_{E'}$	3.2×10^{-17}	cm^2	Literature
Optical cross section for B_1 defect, σ_{B1}	9.4×10^{-18}	cm^2	Data fit
Optical cross section for Ge impurity, σ_{Ge}	1.1×10^{-17}	cm^2	Ge concentration

neutron source. The range may be due to differences in neutron dosimetry calibration or to other uncertainties in the radiation environment, such as the ratio of neutron to gamma dose. To be conservative, we use $M_n = 200$ to predict the NIF final-optics performance.

Predictions for Silica Glass on NIF

The predicted transmission of silica glass as a function of time on NIF is plotted in Fig. 12 for both fused silica type FS1 and fused quartz type FQ1, with an initial condition of $N_{Ge} = 5.7 \times 10^{15}$ cm^{-3} determined from data. The final-focus lens is assumed to be 4.5 cm thick. Thicker lens designs would be expected to have larger absorbance (–log transmission) that is proportional to the thickness. From the predictions in Fig. 12, FS1 is significantly more radiation-resistant than FQ1 at 3ω. Fused silica is expected to have >99% transmission over the 30-year facility lifetime. Fused quartz, however, is expected to drop to a 99% lens transmission within one year, which is undesirable. Fortunately, FS1 is the current baseline material that was assumed in the CDR.

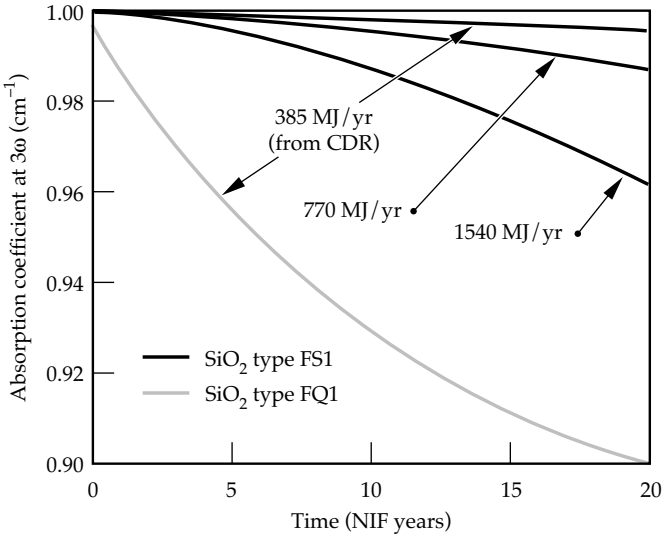

FIGURE 12. Predicted transmission of NIF final-focus lens vs time for fused silica type FS1, such as Corning 7980 or Heraeus Suprasil, and fused quartz type FQ1, such as Heraeus Herasil 1-SV. Predictions for the NIF CDR fusion yield of 385 MJ/year, and for 2 and 4 times that shot rate, are shown for FS1. (70-17-0596-1045pb01)

If the shot rate or target yields on NIF were increased by 2 to 4 times over that assumed in the NIF CDR, (yield rates of 770 and 1540 MJ/yr), the lifetime of the silica final-focus lenses would be reduced. Figure 12 shows our predictions for these shots rates, which lower the effective lifetime to 18 and 9 years for a 2× and 4× increase in yield rate, respectively. This would present an incrementally small increase in the NIF operational cost over the 30-year facility lifetime.

KDP Impurity-Related Radiation Effects

The results of irradiation experiments with both gamma rays and neutrons indicate that only gamma rays have a measurable impact on the UV transmission spectra of KDP at integrated doses relevant to the NIF. Figure 13 shows the spectral results of two representative KDP and KD*P crystals for samples irradiated on the SPR-III (n° and gamma-ray source) and LLNL ^{60}Co (gamma-ray source only). The spectral features observed after similar gamma-ray doses from the two sources are nearly identical in shape and magnitude, demonstrating that the presence of ~1 MeV n° in the SPR-III does not produce observable optical damage in KDP. Direct knock-on neutron collisions will introduce noncrystalline defects; however, they do not appear to introduce optically absorbing species. No changes in refractive index were experimentally observed to within the experimental precision of 10^{-5}. The different spectra in Fig. 13 appear to correlate to the presence of impurities detected by wet chemical analyses of several of the crystals. Most KDP samples give rise to relatively featureless spectra, which show a slight overall increase in absorption (<0.03 cm^{-1} at 3ω). These samples are shown in Fig. 13(a) and (b). The strong absorption band at ~263 nm is typical of As-containing KDP and KD*P, as seen in Figs. 13(c) and (d). Other radiation-sensitive impurities have also been identified and are discussed below.

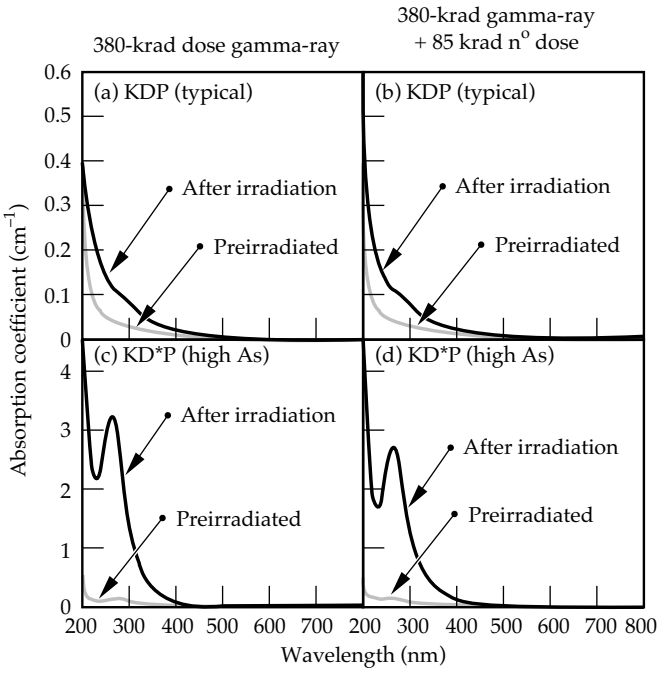

FIGURE 13. KDP and KD*P spectra before and after irradiation with (a) and (c) 380-krad gamma rays, or (b) and (d) 380-kRad gamma rays and 85 krad n°. Spectra are virtually identical with or without the 85-krad neutron dose indicating that gamma-ray damage is expected to dominate the radiation effects for NIF KDP and KD*P. Differences between samples types are due to impurities. All spectra are σ-polarized. (70-17-0596-1046pb01)

In the case of As, where the readily incorporated $(AsO_4)^{3-}$ substitutes isomorphically for the $(PO_4)^{3-}$ group, irradiation by gamma rays turns the anion complex into a color center with a peak absorption at 263 nm, which is presumably $(AsO_4)^{4-}$ based on evidence in the literature.[10,11] To test the correlation of As with the strongly absorbing peak at ~263 nm, we analyzed five samples using inductively coupled plasma (ICP) mass spectroscopy. Figure 14 shows the absorption coefficient of the 263-nm peak as a function of As concentration. In this case, the absorption coefficient was taken from spectra collected after irradiation on the SPR-III (for a gamma-ray dose of 380 krad). A linear regression to the data appears to be a good fit, indicating that As is responsible for the absorbing defect center.

Because As impurities appear to play the most important role in radiation-induced damage in all of the materials studied to date, we recently completed a study to understand the dose dependence of this phenomena. This study allows for predictions of NIF performance based on the integrated gamma-ray dose present in the final optics package as a function of time. Figure 15 is a compilation of results from the SPR-III pulsed nuclear reactor, the LLNL ^{60}Co continuous gamma-ray source, the LLNL pulsed-spallation gamma-ray source (LINAC), and the LANL pulsed spallation n^o and gamma-ray source (LANSCE). All of the data fall onto one curve, indicating that pulse length and radiation spectra do not play a primary role in modifying the radiation-induced damage in KDP. This result can be explained as follows. Gamma rays impart energy to the electronic portion of the atomic structure via Compton scattering. This first produces a ~100-keV electron, for each 1 MeV of initial gamma-ray energy, that then rapidly scatters via cascade e^-–e^- reactions to form multiple ~10-eV electrons. As a consequence, the initial energy of the gamma ray determines the number, rather than the damage characteristics, of final energetic electrons. The ~10-eV electrons next form defects in the material by trapping at precursor sites (e.g., impurities). This simple mechanism is linearly related to the time-integrated, radiation-induced electron density in the conduction band of the material, and does not depend on the initial gamma-ray spectrum or temporal pulse length to first order.

Based on the As precursors described above, we propose a simple mechanism, where

$$\left(AsO_4\right)^{3-} \xrightarrow{\text{gamma rays}} \left(AsO_4\right)^{4-} \xrightarrow{\text{gamma rays}} \left(AsO_3\right)^{2-} + O^{2-} \quad . \tag{8}$$

The $(AsO_4)^{4-}$ species causes the 263-nm absorption shown in Fig. 13(c), whereas the $(AsO_3)^{2-}$ species is believed to have minimal observable absorption. Initial conditions are determined from the concentration of As in the crystal, and all of the As is assumed to be of the form $(AsO_4)^{3-}$. A simple set of coupled rate equations for the concentration of $(AsO_4)^{3-}$, $(AsO_4)^{4-}$, and $(AsO_3)^{2-}$:O^{2-} lead to an analytic solution for the absorption coefficient at 3ω of the form:

$$\alpha = \frac{A_3^0 \sigma_{As} s \beta_{32}}{\left(\beta_{21} - \beta_{32}\right)} \left[\exp\left(-D'\beta_{32}t\right) - \exp\left(-D'\beta_{21}t\right)\right] \quad . \tag{9}$$

The parameters used to fit the data in Fig. 15 using Eq. (9) are defined and quantified in Table 4.

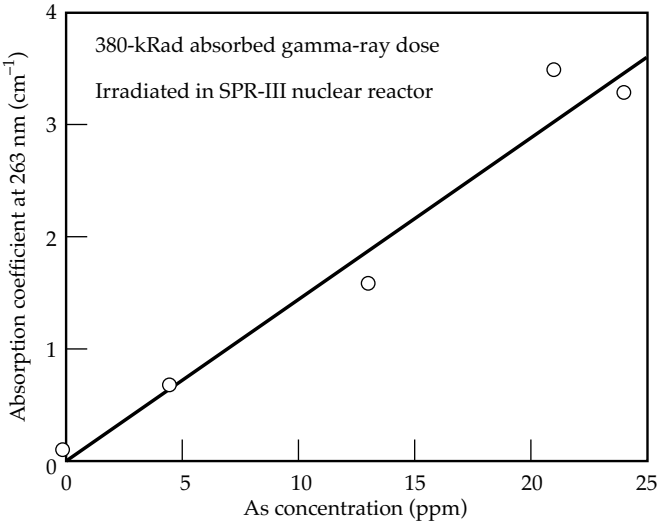

FIGURE 14. Arsenic concentration in ppm by weight vs 380-krad gamma-ray-induced σ-polarized absorption coefficient at 263 nm for several different KDP and KD*P samples. The good linear correlation suggests that As is a precursor for the radiation-induced 263-nm absorption. (70-17-0596-1047pb01)

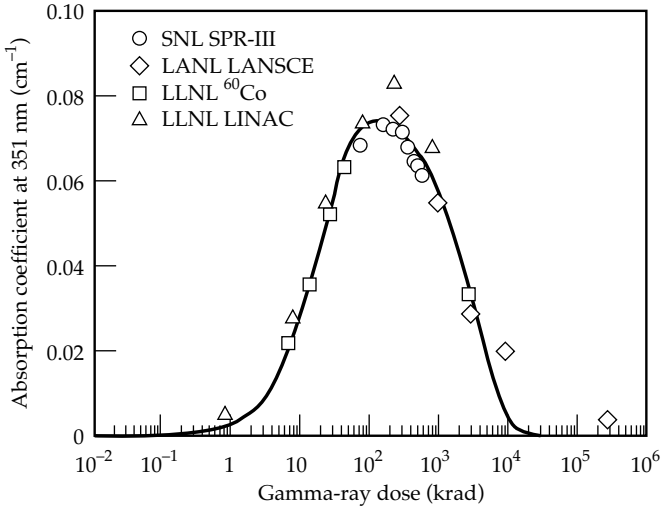

FIGURE 15. Gamma-ray-induced absorption at 3ω (351 nm) as a function of gamma-ray dose. For reference, the NIF is expected to have 160 krad for each decade of operation. Independent data from the source characteristics suggests that the total integrated dose, independent of gamma-ray spectral or temporal characteristics, is adequate for phenomenologically modeling radiation damage in the NIF. (70-17-0596-1048pb01)

From Table 4, we can predict the 3ω transmission of a NIF tripler KD*P crystal, taken to be 0.95 cm thick, for different D–T fusion yields and As impurity concentrations. Figure 16 shows predictions for three different fusion-yield scenarios on the NIF, ranging from a baseline operation of 385 MJ/year to four times this rate (higher gain per shot and/or higher shot rate) for crystals with the same amount of As as a recent crystalline boule grown for the NIF prototype Beamlet Laser System (4.5-ppm As). In any of these cases, the transmission of the tripler drops gradually to 93% within ~1 year. It is clearly undesirable to have this level of loss routinely on the NIF following the first year of full-yield operation. The dotted line in Fig. 16 shows the predicted transmission of a tripler KD*P crystal for 0.5-ppm As. The transmission of this crystal is expected to exceed 99% for the lifetime of the facility. Consequently, 0.5 ppm is the maximum level of As that would be desirable in NIF KD*P triplers. It should be possible to hold the As concentration below this value by using high-purity starting materials.[25]

Impurities other than As could also cause problems in KDP at ppm levels. To test this hypothesis, we irradiated 15 KDP crystals using 14 different impurity dopants and one undoped sample. Results using the SPR-III are summarized in Table 5 and Fig. 17. We found that other impurities—most notably metals, such as Al, Fe, As, Cr, Pb, and V—can lead to significant radiation-induced absorption in KDP. We obtained the concentrations of all the dopants in the crystals, using inductively-coupled plasma mass spectroscopy, in the growth solution and spectra before and after a dose of 1.4×10^{15} n^o/cm^2 and 473 krad of gamma rays. Even thought it is clear that many impurities can cause problems, it is not practical to test the entire periodic table. Consequently, a testing procedure, that uses a readily available radiation source, such as the ^{60}Co source at LLNL, will likely be used on actual starting materials that have been grown into test pieces prior to growth of large boules.

Figure 18 presents typical σ-polarized spectra used to obtain the results in Table 5. The spectra in Fig. 18(a) is for a crystal grown with no deliberate doping, and the resulting change in transmission is minimal in the wavelength region of interest. Figures 18(b) through (d) are for samples doped with Al, Cr, and Pb, respectively. Many of the spectra have absorptions peaked at 266 nm, both before and after irradiation, that look

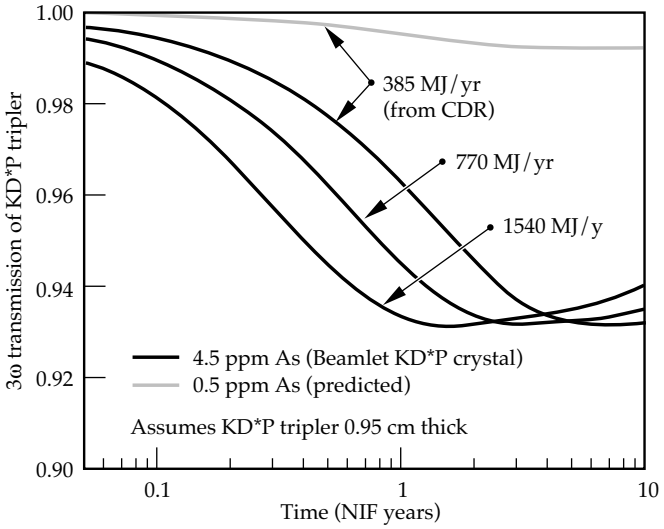

FIGURE 16. Predicted transmission of the NIF KD*P tripler crystal as a function of time for different fusion-yield assumptions and levels of As impurities. (70-17-0596-1049pb01)

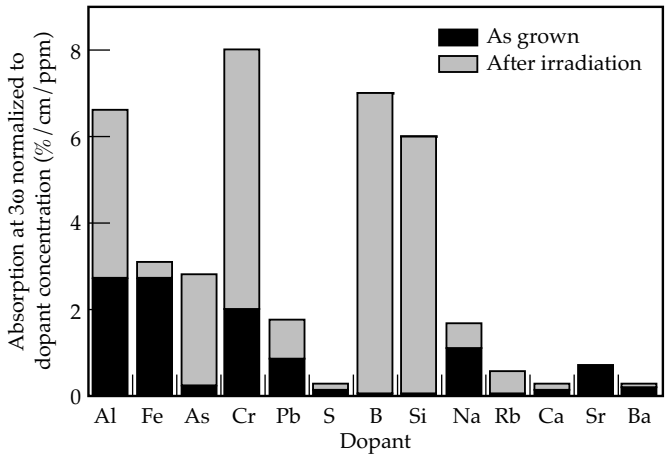

FIGURE 17. Experimental results of irradiating impurity-doped KDP with 473 krad of gamma rays. Absorption coefficients are weighted for concentration in ppm by weight. (70-17-0596-1050pb01)

Parameter	Value	Units	Source
As concentration in Beamlet KD*P boule (LL3LG), A_3°	8.3×10^{16}	cm^{-3}	Measured
Defect optical absorption cross section, σ_{As}	9.3×10^{-19}	cm^2	Data fit
Rate constant for first step in Eq. (8), β_{32}	0.047	1/krad	Data fit
Rate constant for second step in Eq. (8), β_{21}	3.0×10^{-5}	1/krad	Data fit
Gamma ray dose rate, D'	15.9	krad/yr	Ref. 1,19

TABLE 4. Parameters used to model data in Fig. 15 and to predict NIF fused silica final optics performance in Fig. 16.

TABLE 5. Experimental results of deliberately doping KDP with various impurities and irradiating with 1.4×10^{15} n°/cm^2 at 1 MeV equivalent, or 84 krad of neutrons and 473 krad of gamma-rays (Si equivalent). The absorption coefficients are weighted for concentration and were background corrected with a blank sample that showed induced absorptions of 0.0%/cm and 5.9%/cm before and after irradiation, respectively.

Impurity	Concentration in growth solution/crystal (ppm by weight)[25]	Peak absorption wavelength (nm)	Concentration weighted absorption at 3ω before irradiation (%/cm/ppm)	Concentration weighted absorption at 3ω after irradiation (%/cm/ppm)
Al	11/5	266	2.7	6.6
Fe	10/21	<290	2.7	3.1
As	1000/18	263	0.2	2.8
Cr	9/<4	358 and 270	>2	>6
Pb	50/10	<230 and 268	0.8	1.8
V	10/0.9	266	~20	~40
S	250/14	266	0.1	0.3
B	250/<1	266	>7	>7
Si	250/<1	266	>6	>6
Na	1000/15	266	1.1	1.7
Rb	250/26	218	0.6	0.6
Ca	250/34	266	0.1	0.3
Sr	100/0.8	276	0.7	0.7
Ba	100/20	266	0.2	0.3

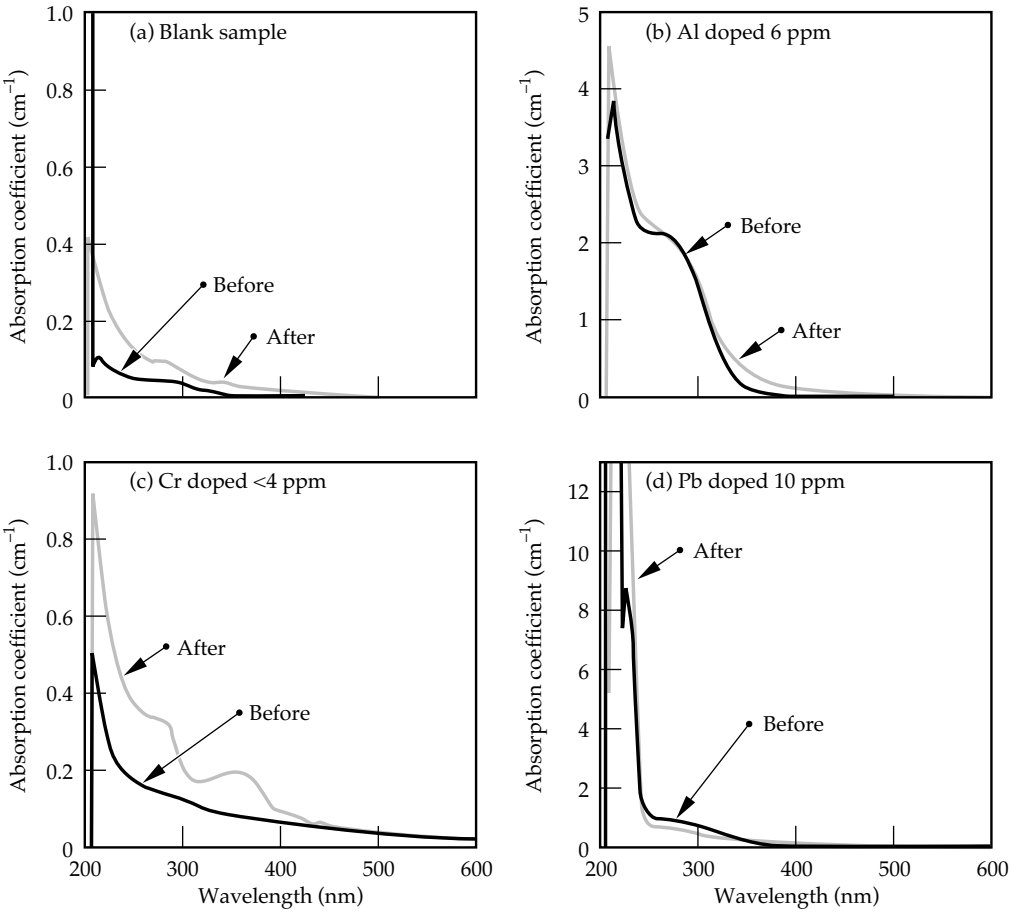

FIGURE 18. Absorption spectra of (a) control sample, and KDP doped with (b) Al, (c) Cr, and (d) Pb before and after irradiation with 1.4×10^{15} n°/cm^2 and 464 krad of gamma rays. (70-17-0596-1051pb01)

virtually identical to that in Fig. 18(b). This transition was observed to be only weakly polarized. Because many different dopants provide the same absorption spectra, this peak appears to be due to an intrinsic vacancy or F center in the KDP lattice induced by the presence of a nearby impurity. [11,26] Some of these dopants have measurable increases in 3ω absorption after irradiation. For example, Al-doped KDP appears to initially have ~3%/cm loss; but following irradiation, it has ~6%/cm loss due to the peak lowering and broadening as shown in Fig. 18(b). This behavior is also observed in general for V, S, B, Si, Na, Rb, Ca, Sr, and Ba dopants, although the magnitude of the effect normalized for concentration seems to vary. Other common impurities in KDP are metals such as Fe, Cr, and Pb. These lead to different absorption features, as noted in Table 3, with varying degrees of impact on 3ω transmission. The transition metals also appear to be more sensitive, in general, to gamma irradiation.

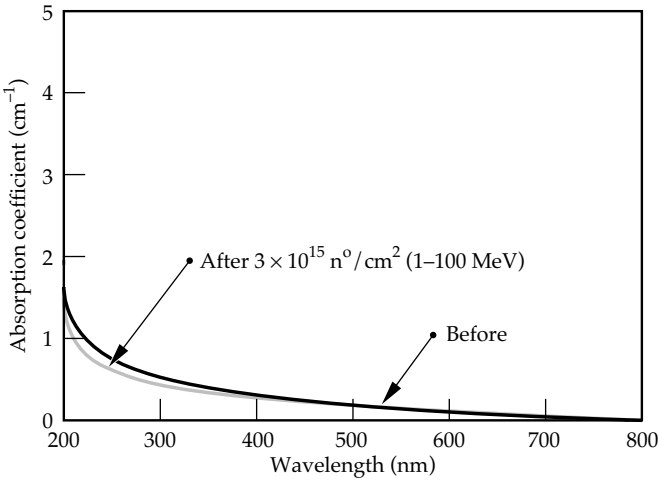

FIGURE 19. Fast-grown KDP sample (LLNL boule LNL-58) before and after irradiation at LANSCE with ns-pulsed, 1- to 100-MeV neutrons and gamma rays with up to ~100 years of the NIF dose at CDR shot rates and assumed yields. (70-17-0596-1052pb01)

High-Energy Neutron Irradiation Experiments

A remarkable outcome of our experiments is the lack of absorption in KDP following irradiation with neutron energies of ~1 MeV. The NIF is expected to produce neutrons that are primarily at 14 MeV directly from the D–T fusion reaction. Consequently, we performed experiments at CEA Sames with 14-MeV n^o irradiation and at LANSCE with 1- to 100-MeV n^o irradiation. Neutron fluxes ranged from 2×10^{14} n^o/cm^2 on Sames to as high as 3×10^{17} n^o/cm^2 on LANSCE. These high-energy neutron irradiations agree with the previous 1-MeV SPR-III neutron-irradiation results in that there are no observable neutron-induced effects in the absorption of the material. Figure 19 shows a typical result for very high-purity KDP irradiated to 3×10^{17} n^o/cm^2. This neutron flux is equivalent to ~100 years of operation on the NIF at 385 MJ/year thermonuclear yield, as assumed in the CDR. The increase in absorption at 3ω was only 5.6 %/cm even after such a large dose. KDP showed significantly less change in UV absorption than fused silica, which is normally assumed to be the "optimal" radiation-resistant optical material. As discussed above, KDP with impurities can have significantly larger induced absorption.

This sample serves as important proof that, with sufficient purity, KDP can withstand the radiation environment on the NIF and have minimal radiation-induced absorption losses at 3ω (<1% per decade of NIF yield). There must, of course, be displacements induced in the crystals from direct-neutron knock-on collisions, but they do not appear to manifest themselves optically at doses relevant to the NIF. This situation may arise from either the lack of natural color centers capable of near-UV or visible absorption, as opposed to vacuum-UV, or possibly from rapid self-annealing of the local displacements at room temperature. Our data suggest that secondary gamma irradiation appears to induce virtually all of the observed damage in KDP.

Summary

We performed a variety of neutron and gamma-ray irradiation experiments in the SNL SPR-III, LANL LANSCE, CEA Sames, and LLNL ^{60}Co and LINAC facilities. These facilities provide complementary sources of gamma rays and neutrons with various energy and pulse formats. We focused on high-energy, penetrating radiation (gamma rays and neutrons) that will propagate through the debris shield and supply a 3-krad dose from neutrons and gamma rays to the NIF final optics for each 20-MJ-equivalent NIF shot. From our experiments and modeling, fused silica (such as Corning 7980 and Heraeus Suprasil) is expected to have <1% loss at 3ω in the final-focus lens after 30 years of use at baseline NIF D–T fusion-yield levels. The optical absorption is due both to neutron-induced displacements and gamma-ray-induced color center formation. Neutrons induce an absorption peak centered at 246 nm, whereas gamma rays introduce absorption peaks centered at 210 and 300 nm in high-purity fused silica and fused quartz, respectively. Increasing the shot rate or yield by 4 times over CDR assumptions is expected to decrease the effective lifetime of the focus lens to 8 years for a ~1% loss. If fused quartz (such as Heraeus Herasil 1)

is used, 1% losses are reached within 1 year for CDR-level fusion yields. Therefore, it is advisable that only radiation-resistant, synthetic fused silica be used for the final-focus lenses.

Neutron collisions do not appear to degrade the optical properties of KDP at NIF-relevant fluences. Gamma rays can cause significant problems if impurities, such as As, are present at ppm levels. For As, which appears to be a common impurity, we constructed a physical picture and measured the quantitative parameters necessary to model the radiation-induced losses expected for KDP and KD*P. We also found that other impurities, such as Al, Fe, As, Cr, Pb, and V, can cause significant problems at ppm concentrations. Assuming these impurities are at acceptable levels, the neutron and gamma-ray damage to KDP arrays should not present a significant problem for more than one decade of NIF operation. Using the LANSCE facility, which has a more severe radiation environment than that expected on the NIF, the purer growths of KDP at LLNL showed virtually no observable degradation (<1%/cm losses) at up to the equivalent dose of ~100 NIF years.

Acknowledgments

We especially thank D. Berry and P. Griffin of SNL for their invaluable efforts in coordinating and performing the SPR-III experiments, and S. Sterbenz and W. Sommer of LANL for their enabling support and insight at LANSCE. W also gratefully thank E. Beriot and P. Schneider of CEA for their coordination of the Sames experiments in France. At LLNL, we thank C. Orth for discussing the neutronic cross sections with us, M. Tobin and J. Latkowski for calculating the radiation source characteristics, T. Diaz de la Rubia for sharing his insights into the neutronic defect mechanisms, and J. Marion, M. Yan, N. Zaitseva, J. Atherton, J. Campbell, and J. DeYoreo for providing the KDP samples and impurity concentrations and for their interest and guidance. We also thank R. Torres for the ICP mass spectroscopy work, and T. Cowan for performing and enabling the e^- spallation experiments. We also thank M. Singh for sharing his RTNS-II data taken in 1987 and more recent insights, and R. Vallene and P. Thelin for sample fabrication.

Notes and References

1. W. A. Bookless and D. Wheatcraft, *Energy & Technology Review*, Lawrence Livermore National Laboratory, Livermore, CA, UCRL-52000-94-12 (1994).
2. C. D. Orth, S. A. Payne, and W. F. Krupke, *Nuclear Fusion* **36** (1), 75–115 (1996).
3. A. Smakula, *J. Opt. Soc. Am.* **40**, 266 (1950).
4. R. A. Weeks and C. Nelson, *J. Am. Ceram. Soc*. **43**, 399 (1960).
5. D. L. Griscom, *J. Ceram. Soc. Japan* **99**, 923 (1991).
6. D. L. Griscom, "Nature of Defects and Defect Generation in Optical Glasses," (SPIE—International Society for Optical Engineering, Bellingham, WA, 1986; *Proc SPIE*, **541**) p. 38–59.
7. M. Rothschild and D. J. Ehrlich, *J. Vac. Sci. Technol. B* **6**, 1 (1988).
8. M. Rothschild, R. B. Goodman, M. A. Hartney, et al., *J. Vac. Sci. Technol. B* **10**, 2989 (1992).
9. D. J. Krajnovich, I. K. Pour, A. C. Tam, et al., *SPIE Proceedings* **1848**, 544 (1992).
10. A. N. Levchenki, V. M. Shulga, and A. O. Doroshenko, *Sov. Phys. Solid State* **32**, 1432 (1990).
11. G. N. Pirogova, Y. V. Coronin, V. E. Kritskaya, et al., *Inorg. Materials* **22**, 97 (1986).
12. C. D. Marshall, J. A. Speth, and S. A. Payne, "Induced Optical Absorption in Gamma and Neutron Irradiated Fused Quartz and Silica," Lawrence Livermore National Laboratory, Livermore, CA, UCRL-JC-122652; submitted to *J. Non-Crystalline Solids* (1995).
13. W. U. Condon and H. Odishaw, *Handbook of Physics* (McGraw-Hill, New York, 1967).
14. D. H. Levy, K. K. Gleason, M. Rothschild, et al., *Appl. Phys. Lett*. **60**, 1667 (1992).
15. M. Guzzi, M. Martini, A. Paleari, et al., *J. Phys. Condensed Matter* **5**, 8105 (1993).
16. H. Imai, K. Arai, J. Isoya, et al., *Phys. Rev. B* **44**, 4812 (1991).
17. R. A. Weeks, *J. Non-Cryst. Solids* **179**, 1 (1994).
18. R. A. Weeks, *J. Am. Ceram. Soc*. **53**, 176 (1970).
19. J. Latkowski, Lawrence Livermore National Laboratory, Livermore, CA, personal communication (1995).
20. *Sandia National Laboratories Radiation Facilities*, (1985), Third Edition, SAND83-0598, Eds. G. A. Zawadzkas, P. A. Kuenstler, and L. M. Choate, available from National Technical Information Service, U. S. Department of Commerce, Springfield, VA.
21. T. Diaz de la Rubia and W. J. Phythian, *J. Nucl. Materials* **191**, 108 (1992).
22. M. S. Livingston and J. P. Blewet, *Particle Accelerators* (McGraw-Hill, New York, 1962).
23. J. Wong, T. Diaz de la Rubia, M. W. Guinan, et al., *J. Nucl. Materials* **212**, 143 (1994).
24. T. Diaz de la Rubia, M. W. Guinan, A. Caro, et al., *Radiation Effects in Solids* **130**, 39 (1994)
25. J. Atherton and J. DeYoreo , Lawrence Livermore National Laboratory, Livermore, CA, personal communication (1995).
26. M. Yang, Lawrence Livermore National Laboratory, Livermore, CA, personal communication (1996).